

# Fe<sub>0.26</sub>Mn<sub>0.26</sub>O<sub>4.5</sub> Binary oxide Nanoparticles as a Promising Adsorbent for Phosphate from Aqueous Medium

Jethave G.N.<sup>1</sup>, Attarde S. B.<sup>1</sup>, Ingle S.T.<sup>1</sup>, Kolate S.S.<sup>2</sup>, Fegade U.A.<sup>2\*</sup>, Mahajan H.A.<sup>3</sup> and Patil A.M.<sup>4</sup>

1. School of Environmental and Earth Sciences, Kavayitri Bahinabai Chaudhari North Maharashtra University, Jalgaon, (MH), INDIA

2. Department of Chemistry, Bhusawal Arts Science and P. O. Nahata Commerce College Bhusawal, (MH), INDIA

3. Department of Chemistry, Smt. G. G. Khadse College Muktainagar, (MH), INDIA

4. Department of Physics, R. C. Patel ACS College, Shirpur (MH), INDIA

\*umeshfegade@gmail.com

## Abstract

The binary oxide nanoadsorbent Fe<sub>0.26</sub>Mn<sub>0.26</sub>O<sub>4.5</sub> (FeMnBONAs) was synthesized by thermal co-precipitation and analyzed by Scanning electron microscopy (FESEM), Infrared spectroscopy (FTIR) and EDX which show that the synthesized sample is an average size 60.5 nm and of Fe, Mn and O the concentrations of Fe, Mn and O, being about 15.03, 14.20 and 70.76% by weight. The results showed that the adsorption of phosphate on FeMnBONAs was pH-dependent. Kinetic data and isothermal adsorption equation followed pseudo-second order and Langmuir respectively. Langmuir isotherm table value derived q<sub>max</sub> 100 and Freundlich isotherm equilibrium and Temkin also show the line diagram. The thermodynamic parameter with the adsorption process  $\Delta G$  is assigned the value of -7.277 kJmol<sup>-1</sup> at 298 K.

**Keywords:** FeMnBONAs, Langmuir isotherm, Freundlich equilibrium, Separation factor.

## Introduction

Several strategies for monitoring the phosphate levels in wastewater have been developed in recent decades<sup>1-4</sup>. Due to its efficiency, cost-effectivity design flexibility, improved selectivity and easy operation, adsorption is one of the most widely used to efficiently eliminate wastewater with inorganic or organic contaminants. The natural adsorbent, bio-synthesized adsorbent and adsorbent are generally widespread in many processes<sup>5,6</sup>. Worldwide, pollution of water is a serious problem. The adsorption of phosphate is necessary both to extract and to restore. The surface adsorption is a phenomenon which results in covalent bonds and electrostatic interactions adsorbing the surface of an adsorbent<sup>7,8</sup>. In contrast, adsorption is unique in that chemical precipitation and biological removal processes can remove impurities over a wide pH and lower levels.

Phosphate is a major nutrient in the aquatic environment in the production of biological organisms. The presence of excessive phosphate was, however, one of the main factors considered for eutrophication and water degradation. Excess phosphate to phytoplankton proliferation and accumulation of algae leads to intense resulting in lack of oxygen and decreased aquatic life<sup>9</sup>.

In recent years, we recognized the receptor to detect metal ions formed in industrial wastewater selectively and sensitively<sup>10-16</sup>. However, in this study, a facile and inexpensive method of synthesis of FeMnBONA was developed and its application to the phosphate removal capacity has been investigated and studied. The study showed that phosphate adsorption kinetics has the best adsorption performance among others and the phosphate removal capacity of FeMnBONA was studied in detail because the isotherm study examines kinetics and equilibrium. In the elimination of phosphates, effects were further explored through various experimental variables such as pH solution, time, concentration etc.

## Material and Methods

**Preparation of FeMnBONAs:** A co-precipitation process at a constant temperature of 60 °C was used to synthesize FeMn nanoparticles of binary oxide with stirring. Next, 7.4 FeCl<sub>2</sub> and 5.6 g MnSO<sub>4</sub> were introduced to 300 ml DDW<sup>10</sup>. Then, at a constant temperature of 60 °C with stirring for up to 2 hours, 30 ml of 5N NaOH were added to the above solution drop wise. The solution color shifted from light brown to black soon after the combining, signaling the development of FeMnBONA. The precipitate was washed to a pH of less than 7.5 and then dried for 24 hours at 100 °C.

**Instrumentation:** FE-SEM (Bruker S-4800 at 15.0 kV) instrument was used for Scanning electron microscopy images. EDX was conducted on the identical instrument in the PM picture size: 500 x 375Mag: 40000 × HV: 15.0 kV. IR spectra (FTIR in the 500-4000 cm<sup>-1</sup> range) of the adsorbent were recorded by FTIR spectrophotometer (model: FT-IR-Bruker). UV-Vis spectra were recorded on the Shimadzu UV-1800 spectrophotometer at room temperature using a quartz cell of 1 cm trajectory length<sup>17</sup>.

**Batch Adsorption Study:** Phosphate adsorption study was performed accordingly<sup>18</sup>. In short, 0.05 g of synthesized FeMnBONAs was added in the 100 ml capacity flask containing 50 ml different concentrations of phosphate solutions. Then the flasks were shaken at rotary shaker with the speed of 200 rpm for 90 minutes at neutral pH and then centrifuged at 2000 rpm for 3 min. Phosphate removal study was done spectrophotometrically at 690 nm. The concentration of phosphate decreased with time due to its adsorption by FeMnBONAs.

The adsorption capacity of phosphate in the adsorption system,  $q_e$ , was calculated by the equation<sup>18,19</sup>

$$q_e = \frac{V(C_0 - C_e)}{m} \quad (1)$$

where  $C_0$  and  $C_e$  are initial and equilibrium concentrations (mg/L) respectively,  $m$  is the mass of the adsorbent (g) and  $V$  is volume of the solution (L)<sup>18</sup>.

## Results and Discussion

**Synthesis of FeMnBONAs and its characterization:** The FeMnBONAs are formulated according to literature<sup>20</sup>. Figure 1 reveals the characteristic SEM pictures of

FeMnBONA. As illustrated in the figure 1(a), the material was observed to be consisting of a significant number of nanostructures. The lower amplification image gives an average particle size of 60.5 nm. EDAX analysis was performed for the observation of the elemental composition of the samples. The analysis revealed that the sample is composed of Fe (15.03%), Mn (14.20%) and O (70.76%) (Figure 2).

The chemical environment of FeMnBONAs was exposed from FTIR analysis and is shown in figure 3. The broad bands at  $1632 \text{ cm}^{-1}$  refer to the O-H stretching frequency of absorbed water. The band at  $1103 \text{ cm}^{-1}$  refers to metal-alloy (Fe-Mn) and bands at  $527$  and  $514 \text{ cm}^{-1}$  are linked to Fe-O bonds due to the presence of ferrite skeleton<sup>21</sup>.

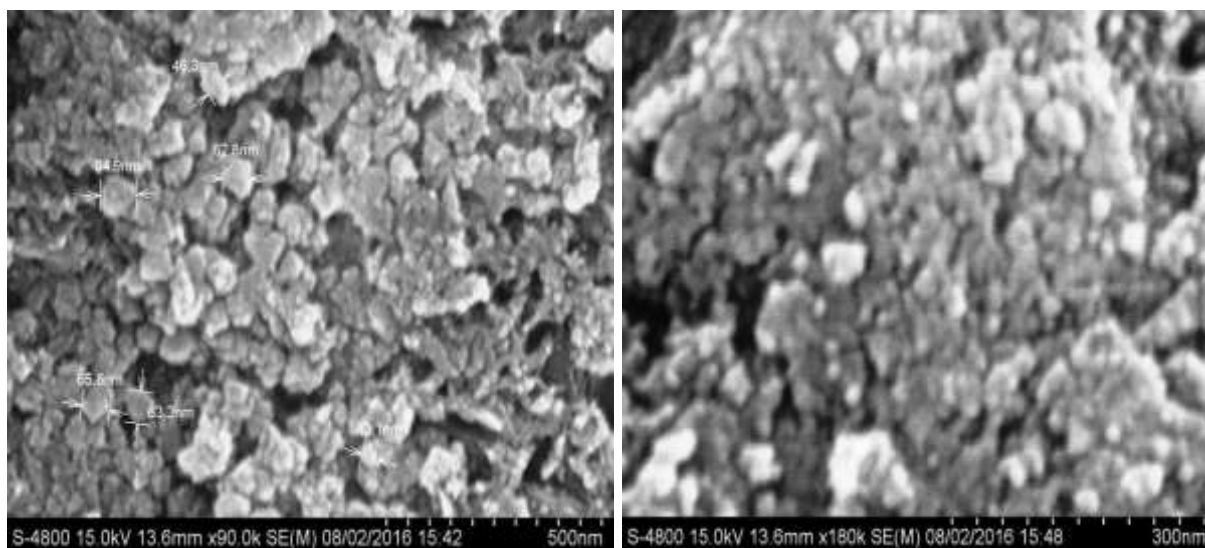


**Fig. 1:** SEM Images FeMnBONAs a) Average particle size 60.5 nm at low magnification and b) high magnification for the closed image of nanoparticle

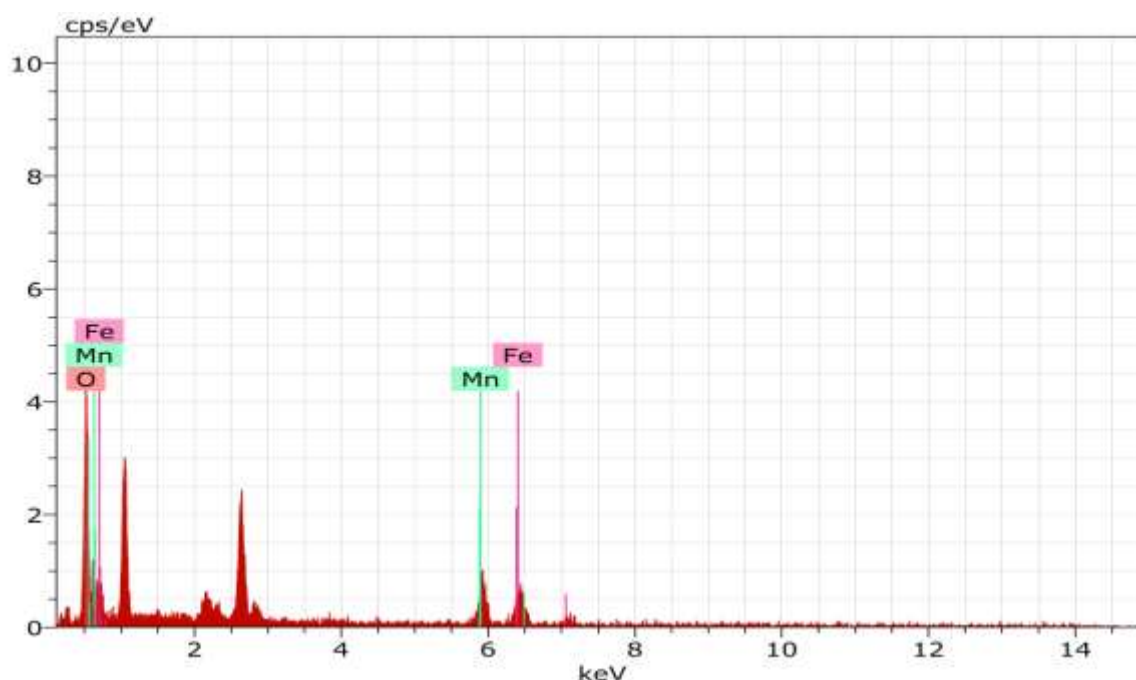


**Fig. 2:** EDX spectra of the FeMnBONAs particles

**Effect of pH solution:** The acid base characteristics of the adsorbent surface depend on the solutions pH. Adsorption tests were performed at a pH range of solution 3.0–7.0. The phosphate uptake of FeMnBONAs is rising with the pH range from 3.0 to 7.0 (Figure 4). The optimal pH is 5.0 for the phosphate adsorption on the adsorbent. FeMnBONAs adsorbs up to 93% of the phosphate at low pH.

On the contrary, when pH is higher than 5.0, the surface charge of this FeMnBONAs will become less positive or even more negative<sup>10</sup>, thereby reducing the adsorption of phosphate because of the electrostatic repulsion between the similar (negative) charged surface of the FeMnBONAs and phosphate<sup>2</sup>.

**Effect of contact time:** The consequence of contact time quite strongly affects the adsorption experiment. So, the

contact time has been varied from 0 to 60 min for the adsorption of 50.0 mg L<sup>-1</sup> phosphate solutions at pH 5.0. A 0.05 g of FeMnBONAs was added into a 50 ppm phosphate solution (50 mL) and the solution was shaken<sup>10</sup>. The aliquot has been taken at a time interval of 5 minutes up to 60 min and absorbance has been taken at 690 nm for determining the phosphate concentration.

The result shows the increases in the % adsorption of phosphate with an increase in time due to its adsorption on FeMnBONAs<sup>10</sup> (Figure 5). Besides this, a decrease in % adsorption of phosphate occurred after 40 min. due to desorption of phosphate. Most of the phosphate (80%) is adsorbed in about 40 minutes. For further operations, the agitation period of 40 min was chosen.

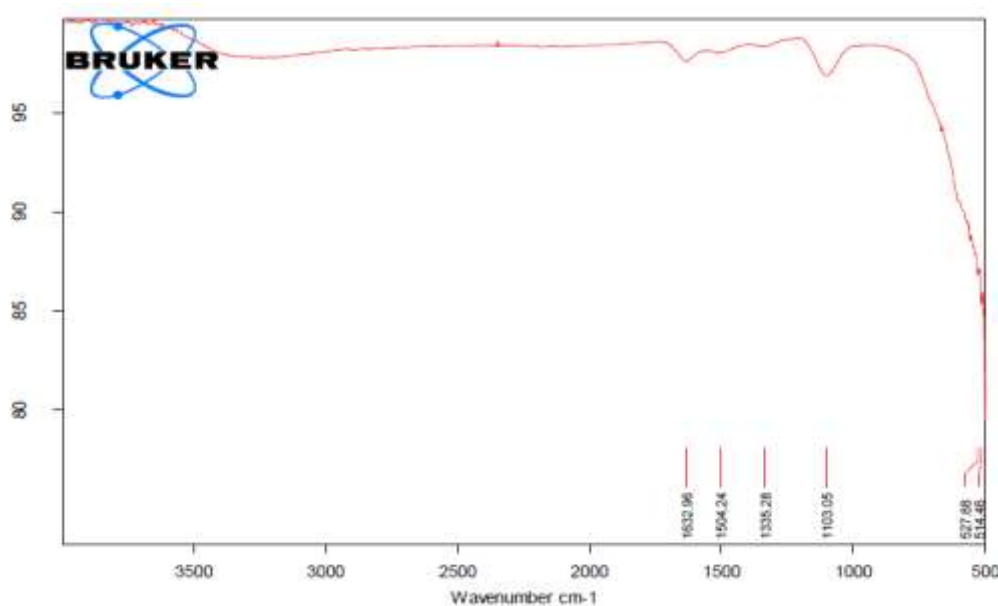


Fig. 3: FTIR spectra of the FeMnBONAs particles

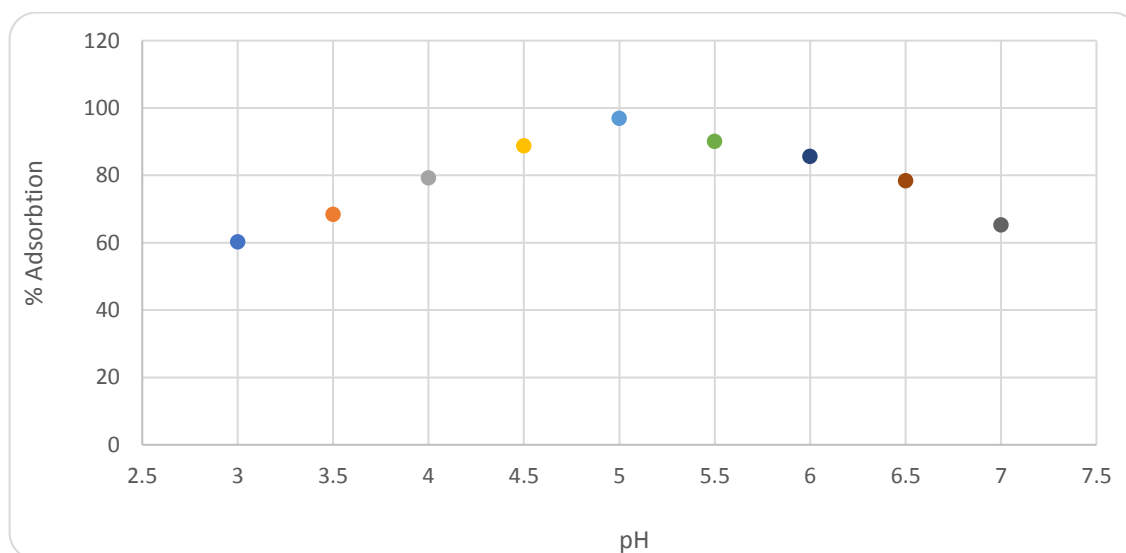


Fig. 4: Effect of initial pH of phosphate solution on removal of CR (FeMnBONAs dosage = 0.05 g, initial phosphate concentration = 50mg/L, stirring time = 90min).

**Effect of Nanoparticle concentration on adsorption:**

During adsorption, the concentration of the adsorbent plays very significant role, as it provides the adequate surface area for phosphate to adsorb on the surface of nanoparticle<sup>10</sup>. In the study, adsorbents differs from 50 mg to 200 mg in the sample. We knew that as we increase the concentration of adsorbent, the active surface area is more available for the adsorption process. The similar trend has been observed in the current experiment. The increase of the adsorption capacity with increasing nanoparticles concentration was performed (Figure 6) until the maximum capacity was reached, which confirmed strong chemical interactions between phosphate and FeMnBONAs.

Larger surface area of FeMnBONAs not only caused higher removal capacities but also enhanced adsorption rate. It was observed that for FeMnBONAs, about 96.88% of the adsorption capacity was reached within 20 minutes of mixing adsorbent and phosphate solution<sup>10</sup>.

**Effect of initial phosphate concentration on adsorption:**

As predicted, cumulative pattern decreases in phosphate

adsorption capability (Figure 7) until the maximum surface area of FeMnBONAs has not been consumed. It was reported that 96 percent of adsorption ability in phosphate solution was obtained as an actual amount of phosphate within minutes of the mixing of adsorbents.

When the phosphate concentration throughout solution was lower, active positions on the adsorbent accompanied much more phosphate ions, but with a rise in initial phosphate concentration, the efficacy of phosphate extraction was decreased by 96% to 50%. This was due to an increase in phosphate concentration whereas the adsorbent dosage was held continuously at 0.2 g.

**Adsorption isotherms modeling:** Langmuir explains the adsorption widely applicable to many sorption methods of gas molecules to metal surfaces. Such adsorbent isotherms believe that adsorption is taking place at certain specific positions of the adsorbent. For the total adsorption efficiency of the complete single-layer coating onto the adsorbent substrate, Langmuir isotherm design was selected.

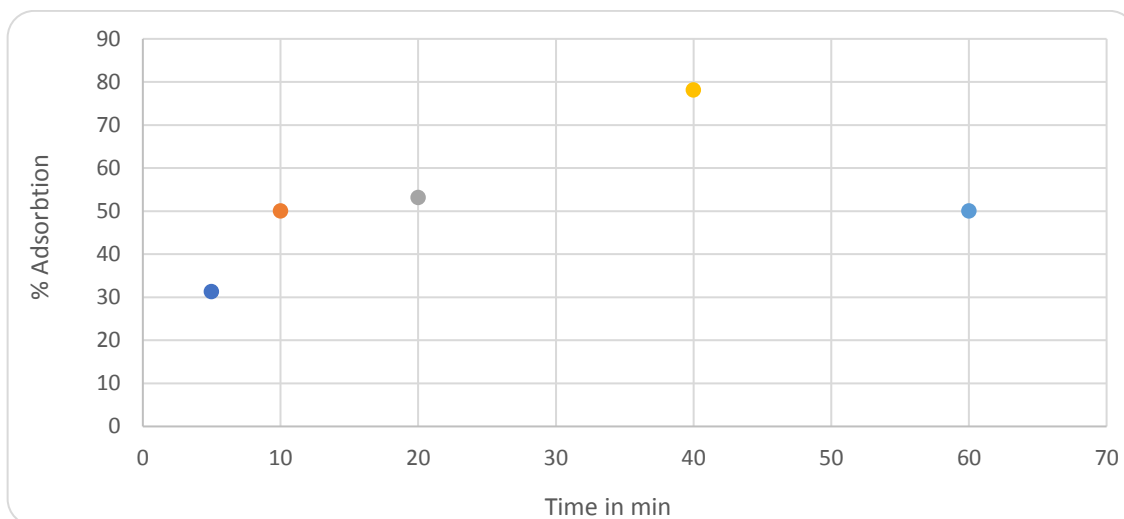


**Fig. 5: Effect of contact time and phosphate concentration on the change in the absorbance for phosphate adsorption at pH 5.0 and 25 °C**

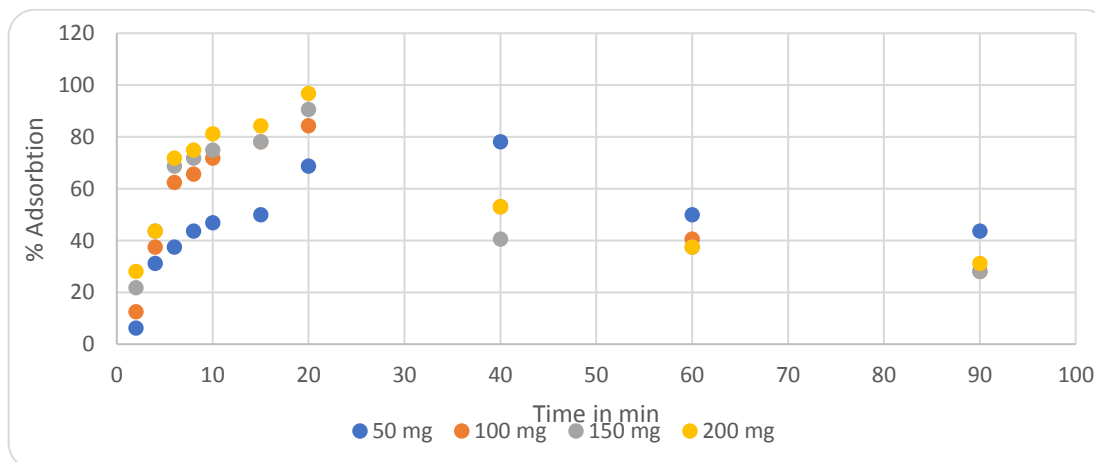


**Fig. 6: Effect of contact time on the adsorption of phosphate to FeMnBONAs at different initial phosphate concentrations (at 25 °C, pH 5)**

When a phosphate group takes place at a surface, there will be no further adsorption at the site (figure 8). The linear Langmuir Equation<sup>10,22</sup> can be shown as supplementary equation 1.

#### Langmuir Isotherm:

$$C_e/q_e = 1/K_L + \alpha L/K_L \times C_e \quad (\text{supplementary equation 1})$$

where  $C_e$  ( $\text{mg L}^{-1}$ ) and  $q_e$  ( $\text{mg g}^{-1}$ ) are the liquid phase concentration and solid phase concentration of adsorbate at equilibrium, respectively;  $K_L$  ( $\text{L g}^{-1}$ ) and  $\alpha L$  ( $\text{L mg}^{-1}$ ) are the Langmuir isotherm constants.

By plotting  $C_e/q_e$  against  $C_e$  (Figure 8), the value of  $K_L$  was obtained from the intercept i.e.  $1/K_L$  and the value of  $\alpha L$  from the slope which was  $\alpha L/K_L$ . The maximum adsorption capacity of the adsorbent ( $q_{\text{max}}$ ) is numerically equal to  $k_L/\alpha L$ .

The Freundlich<sup>23</sup> isotherm is the earliest known relationship describing the adsorption equation. Usually it applies to adsorption onto heterogeneous surfaces with a uniform energy distribution, reversible adsorption and for multilayer adsorption<sup>24</sup> (Figure 9). The commonly used linear form of isotherm is as supplementary equation 2.

#### Freundlich Isotherm:

$$\ln q_e = \ln K_F + 1/n_F \ln C_e \quad (\text{supplementary equation 2})$$

where  $q_e$  is concentration of phosphate adsorbed ( $\text{mg g}^{-1}$ ),  $C_e$  ( $\text{mg L}^{-1}$ ) is the equilibrium phosphate concentration in the aqueous solution and  $K_F$  and  $n$  are constants that are related to the adsorption capacity and the adsorption intensity respectively.

The plot of  $\ln q_e$  versus  $\ln C_e$  was employed to generate the intercept value of  $\ln K_F$  and the slope  $1/n_F$  (Figure 9).

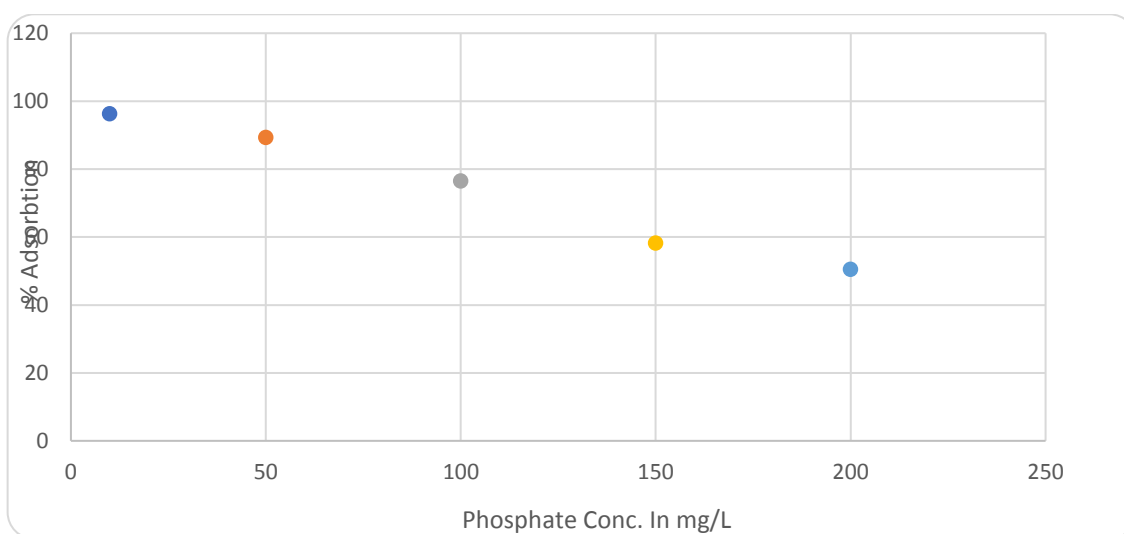


Fig. 7: Effect of contact time on the adsorption of phosphate to FeMnBONAs at different initial phosphate concentrations (at 25 °C, pH 5)

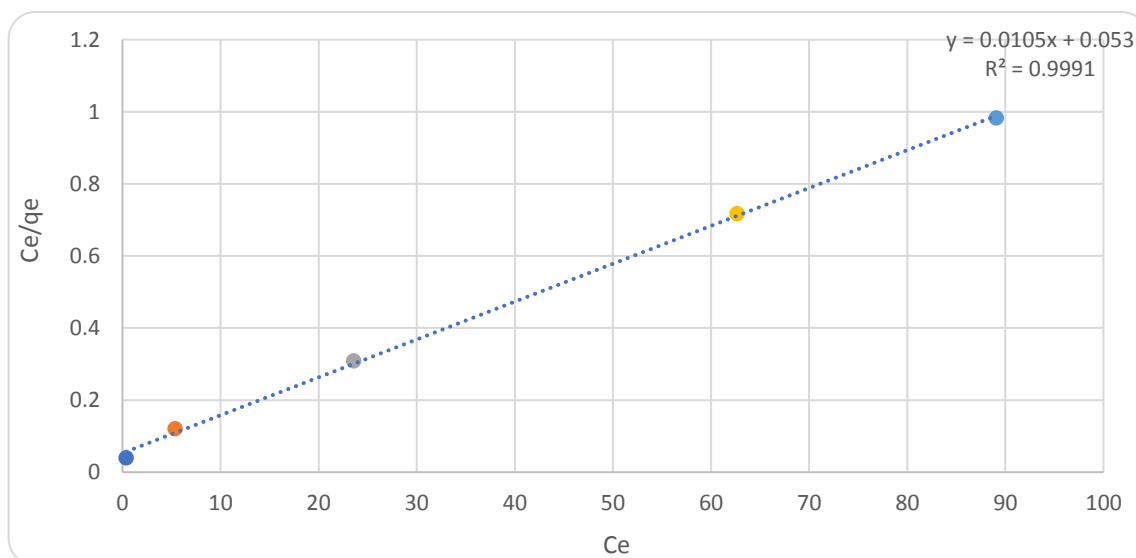
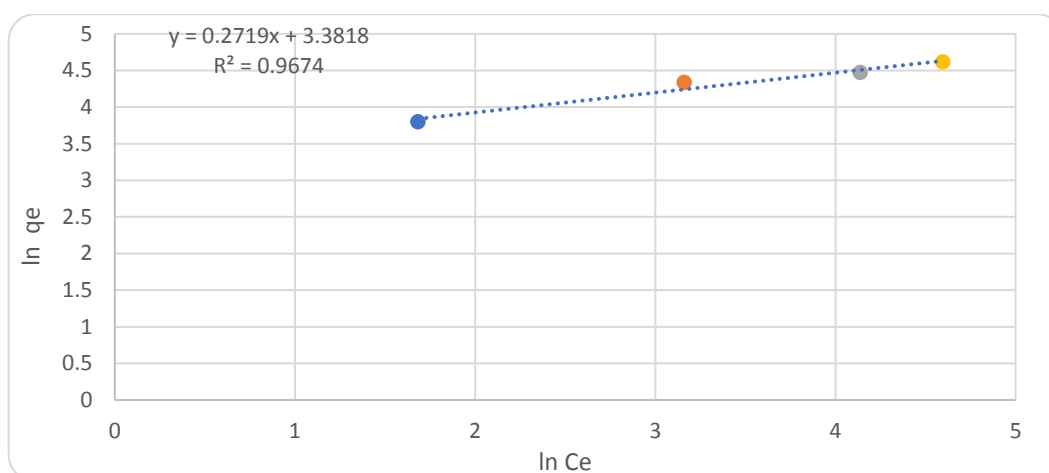


Fig. 8: Langmuir Plot for the adsorption of phosphate onto FeMnBONAs



**Fig. 9: Freundlich Plot for the adsorption of phosphate onto FeMnBONAs**

The Temkin equilibrium isotherm equation was used to describe experimental adsorption data (Figure 10). The heat of the adsorption and the adsorbent–adsorbate interaction by using Temkin isotherm model were evaluated<sup>25,26</sup> (Supplementary equation 3).

#### Temkin Isotherm:

$$q_e = B_1 \ln KT + B_1 \ln C_e \quad (\text{supplementary equation 3})$$

where  $C_e$  is the equilibrium concentration (mg/L),  $q_e$  is the amount adsorbed at equilibrium (mg/g),  $B$  is the Temkin constant related to heat of the adsorption ( $\text{J mol}^{-1}$ ),  $T$  is the absolute temperature (K),  $R$  is the universal gas constant ( $8.314 \text{ J mol}^{-1} \text{ K}^{-1}$ ),  $KT$  is the equilibrium binding constant ( $\text{L mg}^{-1}$ ).

The values and correlation coefficient of the Temkin constants are smaller than the Langmuir. The strongest analogy of experimental data is therefore the Langmuir isotherm which shows that the adsorption under analysis is monolayer or chemical adsorption. The Temkin model's correlation coefficients  $R^2$  were less but comparable to those of the Langmuir and Freundlich equations that describe the Temkin model's application to the adsorption of phosphate on FeMnBONAs.

**Separation factor  $R_L$ :** The basic properties of the Langmuir isotherm can be expressed by describing the supplementary formula 4 in a dimensionless constant named separation variable ( $R_L$ )<sup>26</sup>. The  $R_L$  value was noted to be within 0–1 which confirmed that the phosphate was well adsorbed. The calculated  $R_L$  values at different initial phosphate concentration are reported in figure 11. Further  $R_L$  values indicated that adsorption at lower phosphate levels was more beneficial.

#### Separation Factor:

$$R_L = 1/(1 + \alpha_L C_0) \quad (\text{supplementary equation 4})$$

where  $C_0$  is the initial concentration ( $\text{mg L}^{-1}$ ) and  $\alpha_L$  is the Langmuir constant related to the energy of adsorption ( $\text{Lmg}^{-1}$ ). The value of  $R_L$  indicates the shape of the isotherms to be either unfavorable ( $R_L > 1$ ), linear ( $R_L = 1$ ), favorable ( $0 < R_L < 1$ ) or irreversible ( $R_L = 0$ ).

**Adsorption Thermodynamic parameters:** Temperature-dependent adsorption isotherms are used for the measurement of thermodynamic parameters<sup>27</sup> including enthalpy change ( $\Delta H^\circ$ ), entropy change ( $\Delta S^\circ$ ) and Gibbs free energy change ( $\Delta G^\circ$ ) for phosphate adsorption on FeMnBONAs. The slope and intercept of the chart  $\ln K_L$  vs  $1/T$  can be used to calculate values of  $\Delta H^\circ$  and  $\Delta S^\circ$  by using the supplementary equation 5<sup>28</sup>.

#### Thermodynamic Parameters:

$$\ln K_L = \Delta S^\circ/R - \Delta H^\circ/RT \quad (\text{supplementary equation 5})$$

where  $R$  ( $8.314 \text{ Jmol}^{-1}\text{K}^{-1}$ ) is the ideal gas constant, and  $T$  (K) is the temperature in Kelvin.

The value of  $\Delta G^\circ$  for specific adsorption was calculated based on the basic thermodynamic formula (supplementary equations 6 and 7). Table no. 2 lists the values derived from equations 6 and 7. The assessment of thermodynamic parameters gives an insight into the phosphate adsorption mechanism to FeMnBONAs. The change in free energy for adsorption of phosphate onto FeMnBONAs nanoparticles is  $-7.277 \text{ KJmol}^{-1}$  at 298 K; the potential to adsorb phosphate was improved by an improvement in the solution temperature. An increase of mobility of the phosphate molecules may result in an improving interaction with the binding sites of adsorbent surface due to the increased adsorption capacity at higher temperatures. The low value of  $\Delta H^\circ$  indicates that phosphate and FeMnBONAs nanoparticles interactions are weak.

$$\Delta G^\circ = RT \ln K_L \quad (\text{supplementary equation 6})$$

$$\Delta G^\circ = \Delta H^\circ - T\Delta S^\circ \quad (\text{supplementary equation 7})$$

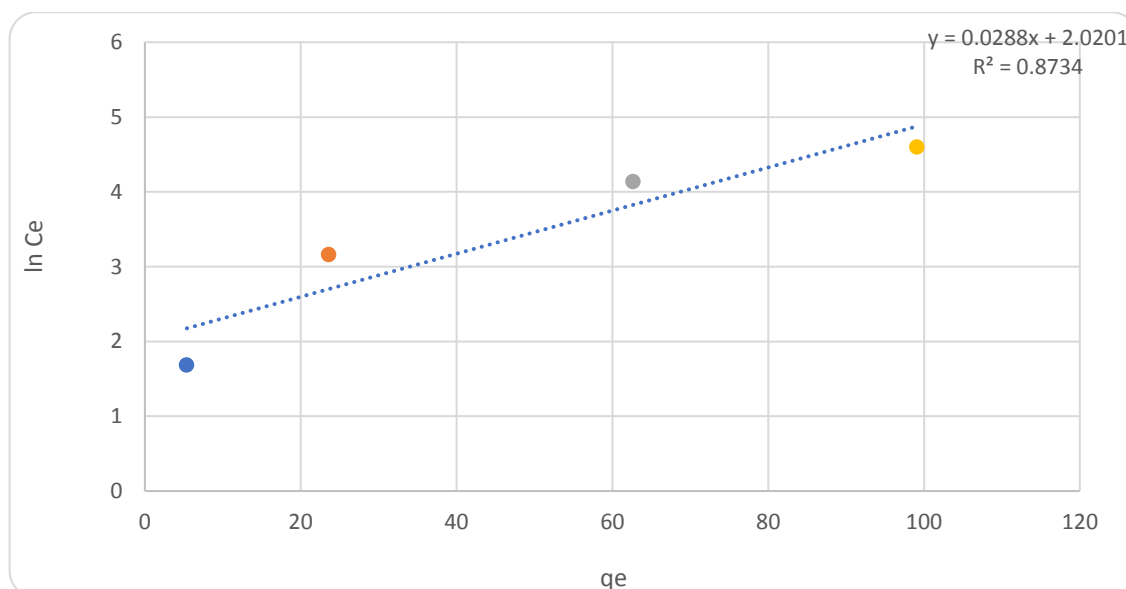


**Fig. 10: Tempkin model Plot for the adsorption of Phosphate onto FeMnBONAs at 25 °C**

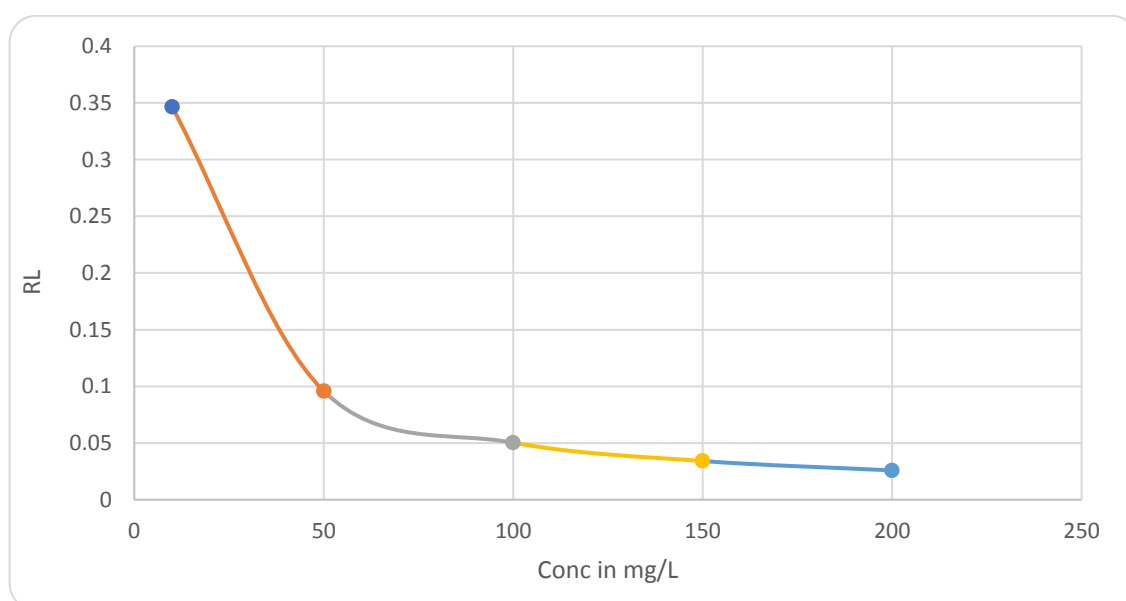


**Fig. 11: Separation factor for the adsorption of Phosphate onto FeMnBONAs at 25 °C**

The value of  $\Delta G^\circ$  is negative and the absolute value decreases with an increase in temperature, suggesting that the adsorption of phosphate on the FeMnBONAs nanoparticles is spontaneous<sup>27</sup>. The negative value of enthalpy change ( $\Delta H^\circ$ ) indicates exothermic adsorption consistent with the adsorption results. The decline of a randomness on the solid-solution interface throughout the adsorption process was confirmed by negative value in the change in entropy ( $\Delta S^\circ$ ).

**Regeneration of FeMnBONAs:** The adsorption-desorption process was replicated three times to explore the reusability of FeMnBONAs and the results indicated that HCl (0.1 M) is an effective medium for FeMnBONAs desorption and reusability studies<sup>10</sup>. It is shown that after the 3<sup>rd</sup> adsorption-desorption cycle in figure 13, the adsorption capacity of FeMnBONAs remained above 92 percent. It can,

therefore, be claimed that FeMnBONAs can be easily renewed with HCl solution which can be used frequently as effective adsorbents for the practical treatment of wastewater<sup>29</sup>.

**Industrial applications:** In the current work, synthesized  $\text{Fe}_{0.26}\text{Mn}_{0.26}\text{O}_{4.5}$  adsorbent is applied to phosphate removal of industrial waste samples. The variation in removal percentage, particularly at higher sample volume and concentration of phosphate molecule must not exceed  $\pm 5\%$  to suppose that the method can be applied as pilot plant<sup>25</sup>. Two effluent streams were used to examine the productivity of the present adsorbents for removing phosphate from real effluents. Thereafter, in our experiments, 50 mL of concentrated wastewater was diluted to 500 mL and optimized procedure was carried out.

**Table 1**  
The data deduced from Langmuir, Freundlich and Tempkin Isotherm plot

Langmuir Isotherm		Freundlich Isotherm		Tempkin Isotherm	
$1/K_L$	0.053	$\ln K_f$	1.468	B	0.028
$q_{max} = K_L/\alpha_L$	100	$1/nf$	0.271	$B \ln KT$	2.02
$R^2$	0.999	$R^2$	0.967	$R^2$	0.873

**Table 2**  
Thermodynamic parameters for phosphate adsorption onto FeMnBONAs nanoparticles

Temp (K)	$\Delta G^\circ$ (kJ mol <sup>-1</sup> )	$\Delta H^\circ$ (kJ mol <sup>-1</sup> )	$\Delta S^\circ$ (J mol <sup>-1</sup> K <sup>-1</sup> )
298	-7.277	-31.244	-2033.604
308	-7.588		
318	-7.902		

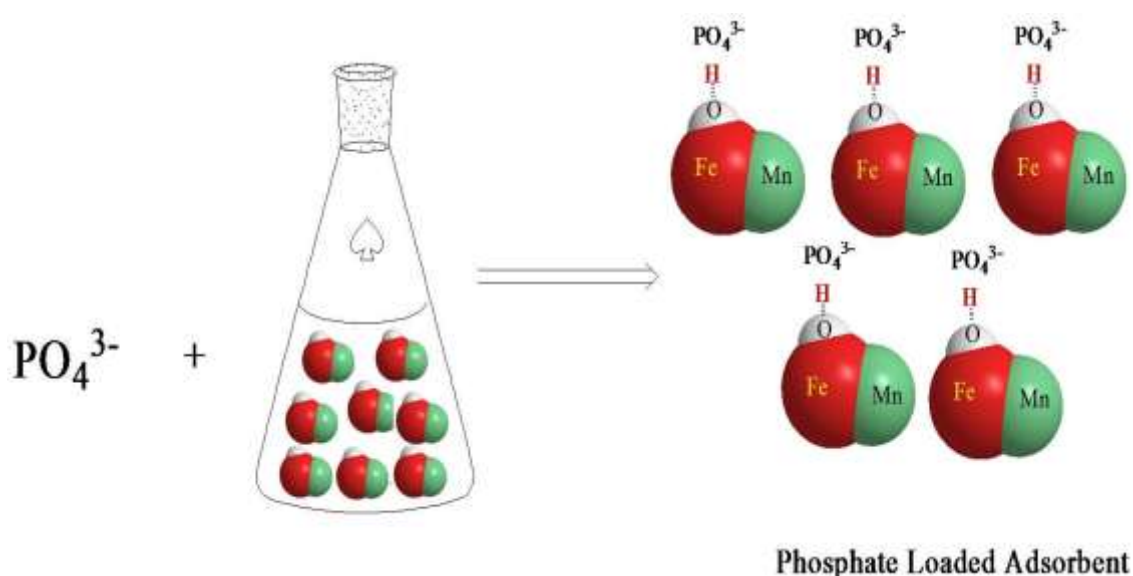


**Fig. 12:** Schematic representation of  $PO_4^{3-}$  adsorption on FeMnBONAs

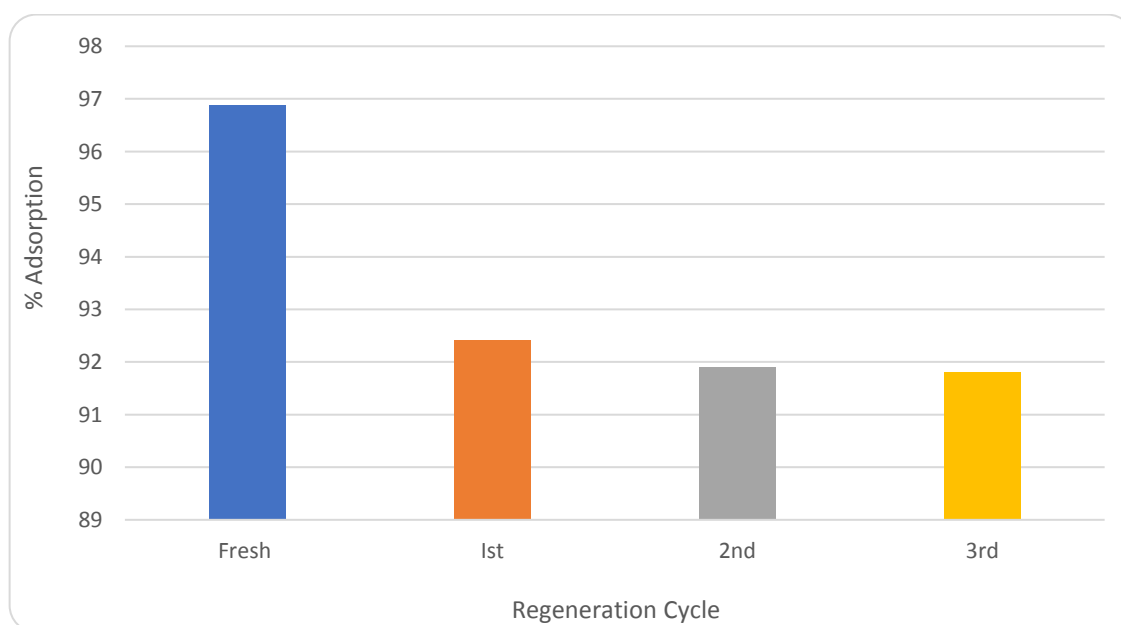


**Fig. 13:** Influence of regeneration of FeMnBONAs by acid on adsorption capacity

**Table 3**  
**Direct application of Fe<sub>0.26</sub>Mn<sub>0.26</sub>O<sub>4.5</sub> on waste of laboratory and industrial waste samples**

Sample	Sample No.	Initial Phosphate concentration (mgL <sup>-1</sup> )	Final Phosphate concentration (mgL <sup>-1</sup> )	Removal (%)	Average	RSD
Waste of Laboratory	1	50	1.44	96.33	96.25	0.83
	2		1.55	95.41		
	3		1.54	97.01		
Industrial waste sample	1		1.91	94.21	93.54	0.92
	2		1.59	93.85		
	3		1.775	92.56		

The result shows that the significant adsorption of phosphate occurs when the volume is large but again we carried out experiment at high volume and concentration<sup>25</sup>. Over 95% of phosphate reduction was achieved in all the methods tested using 200 mg of adsorbent for 1.5 h. Table 3 shows all the experimental conditions and results. Over 90 percent of phosphate removal was found to have been achieved in most cases. It indicates the adsorbent's utility in eliminating phosphate.

### Conclusion

High-performance FeMnBONAs nanoparticles were efficiently prepared by using a high-efficient and simple method and is used as adsorbent for phosphate removal. Its high magnification SEM image shows average particle size 60.5 nm and EDAX analysis was performed for the observation of the elemental composition of the samples. The analysis revealed that the sample is composed of Fe (15.03%), Mn (14.20%) and O (70.76%).

Langmuir isotherm model fits experimental data quite accurately than Freundlich model. The total adsorption efficiency is 100 mg g<sup>-1</sup>, far better than many other nano adsorbents for FeMnBONAs. Thermodynamic parameter  $\Delta G^\circ$  indicates a value -7.277 k J mol<sup>-1</sup> for the adsorption method. The present study will provide a deeper explanation of the synthesis and use of Fe-Mn nanoparticles in water treatment.

### Acknowledgement

This work was supported by the Council of Scientific and Industrial Research (CSIR), India, for financial support under CSIR-SRF (Direct) fellowship scheme awarded to the first author Mr. Ganesh N. Jethave (Ack. No. 122066/2K17/1).

### References

- Yang W., Yu Z., Pan B., Lv L. and Zhang W., Simultaneous organic/inorganic removal from water using a new nanocomposite adsorbent: A case study of p-nitrophenol and phosphate, *Chem Eng J.*, doi:10.1016/j.cej.2015.01.051, **268**, 399-407 (2015)
- Song L., Huo J., Wang X., Yang F., He J. and Li C., Phosphate adsorption by a Cu(II)-loaded polyethersulfone-type metal affinity membrane with the presence of coexistent ions, *Chem Eng J.*, doi:10.1016/j.cej.2015.08.1462016, **284**, 182-193 (2016)

- Lalley J., Han C., Li X., Dionysiou D.D. and Nadagouda M.N., Phosphate adsorption using modified iron oxide-based sorbents in lake water: Kinetics, equilibrium and column tests, *Chem Eng J.*, doi:10.1016/j.cej.2015.08.114, **284**, 1386-1396 (2016)
- Chen J. et al, Efficient removal of phosphate by facile prepared magnetic diatomite and illite clay from aqueous solution, *Chem Eng J.*, doi:10.1016/j.cej.2015.11.028, **287**, 162-172 (2016)
- Eljamal O., Khalil A.M.E., Sugihara Y. and Matsunaga N., Phosphorus removal from aqueous solution by nanoscale zero valent iron in the presence of copper chloride, *Chem Eng J.*, doi:10.1016/j.cej.2016.02.052, **293**, 225-231 (2016)
- Lu J., Liu D., Hao J., Zhang G. and Lu B., Phosphate removal from aqueous solutions by a nano-structured Fe-Ti bimetal oxide sorbent, *Chem Eng Res Des.*, doi:10.1016/j.cherd.2014.05.001, **93**, 652-661 (2015)
- Acelas N.Y., Martin B.D., López D. and Jefferson B., Selective removal of phosphate from wastewater using hydrated metal oxides dispersed within anionic exchange media, *Chemosphere*, doi:10.1016/j.chemosphere.2014.02.024, **119**, 1353-1360 (2015)
- Jia Z., Wang Q., Liu J., Xu L. and Zhu R., Effective removal of phosphate from aqueous solution using mesoporous rodlike NiFe<sub>2</sub>O<sub>4</sub> as magnetically separable adsorbent, *Colloids Surfaces A Physicochem Eng Asp.*, doi:10.1016/j.colsurfa.2013.07.025, **436**, 495-503 (2013)
- Wu D., Shen Y., Ding A., Qiu M., Yang Q. and Zheng S., Phosphate removal from aqueous solutions by nanoscale zero-valent iron, *Environ Technol (United Kingdom)*, doi:10.1080/09593330.2013.786103, **34(18)**, 2663-2669 (2013)
- Fegade U., Jethave G., Su K.Y., Huang W.R. and Wu R.J., An multifunction Zn<sub>0.3</sub>Mn<sub>0.4</sub>O<sub>4</sub> nanospheres for carbon dioxide reduction to methane via photocatalysis and reused after five cycles for phosphate adsorption, *J Environ Chem Eng.*, doi:10.1016/j.jece.2018.02.040, **6(2)**, 1918-1925 (2018)
- Fegade U., Sahoo S.K., Attarde S., Singh N. and Kuwar A., Colorimetric and fluorescent "on-off" chemosensor for Cu<sup>2+</sup> in semi-aqueous medium, *Sensors Actuators, B Chem.*, doi:10.1016/j.snb.2014.06.033, **202**, 924-928 (2014)
- Fegade U.A., Sahoo S.K., Singh A., Singh N., Attarde S.B. and Kuwar A.S., A chemosensor showing discriminating fluorescent response for highly selective and nanomolar detection of Cu<sup>2+</sup> and Zn<sup>2+</sup> and its application in molecular logic gate, *Anal Chim Acta*,

doi:10.1016/j.aca.2015.02.051, **872**, 63-69 (2015)

13. Fegade U. et al, A selective and discriminating noncyclic receptor for  $\text{HSO}_4^-$  ion recognition, *RSC Adv.*, doi:10.1039/c3ra47935h, **4(29)**, 15288-15292 (2014)

14. Fegade U. et al, "Turn-on" fluorescent dipodal chemosensor for nano-molar detection of  $\text{Zn}^{2+}$ : Application in living cells imaging, *Talanta*, doi:10.1016/j.talanta.2014.03.002, **125**, 418-424 (2014)

15. Fegade U., Tayade S., Chaitanya G.K., Attarde S. and Kuwar A., Fluorescent and chromogenic receptor bearing amine and hydroxyl functionality for iron (III) detection in aqueous solution, *J Fluoresc.*, doi:10.1007/s10895-014-1358-3, **24(3)**, 675-681 (2014)

16. Fegade U., Saini A., Sahoo S.K., Singh N., Bendre R. and Kuwar A., 2,2'-(Hydrazine-1,2-diylidenedimethylidene)bis(6-isopropyl-3-methylphenol) based selective dual-channel chemosensor for  $\text{Cu}^{2+}$  in semi-aqueous media, *RSC Adv.*, doi:10.1039/c4ra04656k, **4(75)**, 39639-39644 (2014)

17. Jethave G., Fegade U., Rathod R. and Pawar J., Dye Pollutants removal from Waste water using Metal Oxide Nanoparticle embedded Activated Carbon: An Immobilization study, *J Dispers Sci Technol.*, doi:10.1080/01932691.2018.1472016, **40(4)** (2019)

18. Fegade U., Jethave G., Su K.Y., Huang W.R. and Wu R.J., An multifunction  $\text{Zn}_{0.3}\text{Mn}_{0.4}\text{O}_4$  nanospheres for carbon dioxide reduction to methane via photocatalysis and reused after five cycles for phosphate adsorption, *J Environ Chem Eng.*, doi:10.1016/j.jece.2018.02.040, **6(2)** (2018)

19. Jethave G., Fegade U., Attarde S. and Ingle S., Facile synthesis of Lead Doped Zinc-Aluminum Oxide Nanoparticles (LD-ZAO-NPs) for efficient adsorption of anionic dye: Kinetic, isotherm and thermodynamic behaviors, *J Ind Eng Chem.*, doi:10.1016/j.jiec.2017.04.038, **53**, 294-306 (2017)

20. Jethave G. et al, An Multifunction  $\text{Zn}_{0.3}\text{Mn}_{0.4}\text{O}_4$  Nanospheres for Carbon dioxide Reduction to Methane via Photocatalysis and Reused after fifth cycles for Phosphate Adsorption, *J Environ*

*Chem Eng.*, doi:https://doi.org/10.1016/j.jece.2018.02.040 (2018)

21. IWA Publishing, <https://iwaponline.com/>, Accessed February 4 (2020)

22. Langmuir I., The constitution and fundamental properties of solids and liquids, PART I, Solids, *J Am Chem Soc.*, doi:10.1021/ja02268a002, **38(11)**, 2221-2295 (1916)

23. Spencer Hartley G., Cook A.H., Zechmeister L., Frehden O. and Fischer Jrgens P., The Adsorption of Cis-and Trans-Azobenzene, UTC 1937, <https://pubs.acs.org/sharingguidelines> (2020)

24. Home ScholarBank@NUS, <https://scholarbank.nus.edu.sg/> (2020)

25. Home - Springer, <https://link.springer.com/> (2020)

26. Weber T.W. and Chakravorti R.K., Pore and solid diffusion models for fixed-bed adsorbers, *AIChE J.*, doi:10.1002/aic.690200204, **20(2)**, 228-238 (1974)

27. Zeng S., Duan S., Tang R., Li L., Liu C. and Sun D., Magnetically separable  $\text{Ni}_{0.6}\text{Fe}_{2.4}\text{O}_4$  nanoparticles as an effective adsorbent for dye removal: Synthesis and study on the kinetic and thermodynamic behaviors for dye adsorption, *Chem Eng J.*, doi:10.1016/j.cej.2014.07.093, **258**, 218-228 (2014)

28. Zhu H.Y., Jiang R., Fu Y.Q., Jiang J.H., Xiao L. and Zeng G.M., Preparation, characterization and dye adsorption properties of  $\gamma\text{-Fe}_2\text{O}_3/\text{SiO}_2/\text{chitosan}$  composite, *Appl Surf Sci.*, doi:10.1016/j.apsusc.2011.09.045, **258(4)**, 1337-1344 (2011)

29. Jethave G., Fegade U., Attarde S. and Ingle S., Facile synthesis of Lead Doped Zinc-Aluminum Oxide Nanoparticles (LD-ZAO-NPs) for efficient adsorption of anionic dye: Kinetic, isotherm and thermodynamic behaviors, *J Ind Eng Chem.*, doi:10.1016/j.jiec.2017.04.038, **53** (2017).

(Received 04<sup>th</sup> February 2020, accepted 12<sup>th</sup> April 2020)